Lab 6 Report

Analyzing the Aerodynamic Performance of Flexible Finite Wings

Prepared by: Team 13 Black
Timothy Anderson (ande1389@purdue.edu)
Glenn Brock (gbrock@purdue.edu)
Justin Dang (dang56@purdue.edu)
Sarah Govostis (sgovosti@purdue.edu)
Jaden Hernandez (herna653@purdue.edu)
Charlotte Fellows (cfellow@purdue.edu)
Abby Frank (frank106@purdue.edu)

School of Aeronautics and Astronautics,
Purdue University
701 W. Stadium Ave.
West Lafayette, IN 47907

Date: 2025-04-23

Submitted to: Prof. Sally Bane and Tsung Min (Dylan) Hsieh

1 Introduction

In recent years, there has been a growing interest in the use of flexible materials in aerospace applications, particularly in the development of small-scale unmanned aerial vehicles and remote-control aircraft. One of the primary motivations behind this trend is the pursuit of increased durability and impact resistance through the use of elastomeric materials like thermoplastic polyurethane (TPU). These materials have shown promise in improving impact resistance and extending service life, making them especially attractive for aircraft operating in uncertain or variable environments.

Beyond durability, flexible materials present a unique opportunity to alter wing shape during flight passively. This concept draws inspiration from nature, where birds can actively adjust the camber and shape of their wings to adapt to varying flight conditions. Engineers have begun exploring how similar effects can be achieved through material deformation rather than active control surfaces, with the potential to reduce mechanical complexity and weight.

Despite this potential, there remains a lack of comprehensive data on how wing flexibility affects aerodynamic performance, particularly in terms of lift and drag generation. It is hypothesized that while flexibility may offer certain advantages at lower angles of attack or during dynamic maneuvers, excessive deformation could lead to unfavorable changes in wing geometry, such as increased form drag or reduced lift effectiveness. Understanding these trade-offs is crucial for evaluating the viability of flexible-wing designs in real-world applications.

To investigate this, four finite wings based on the symmetric NACA 0012 airfoil were 3D printed using varying material properties—from stiff polylactic acid (PLA) to more flexible thermoplastic polyurethane (TPU) filament with different infill percentages. The performance of each wing was evaluated in a subsonic wind tunnel at multiple angles of attack to measure how flexibility influences aerodynamic force production.

The lift (L) and drag (D) forces on a wing can be described by the following equations:

$$L = \frac{1}{2}\rho V^2 S C_L \tag{1}$$

$$D = \frac{1}{2}\rho V^2 S C_D \tag{2}$$

Where:

- ρ is the air density
- V is the free-stream velocity
- S is the surface area of the wing
- C_L and C_D are the lift and drag coefficients, respectively.

For a symmetric airfoil like the NACA 0012, the lift coefficient generally increases linearly with angle of attack in the linear region of the lift curve, and stall occurs at a relatively high angle of attack at roughly 16°. However, this linear relationship may be disrupted for flexible wings due to shape deformation, altering both the effective camber and flow separation characteristics. It is assumed in this experiment that flow is steady and incompressible, and that all wings are mounted under similar conditions with consistent wind tunnel speed. Additionally, it is assumed that the force balance system is properly calibrated and that the wings are clamped rigidly at their root to prevent extraneous movement not due to airflow. This study aims to bridge the gap between structural flexibility and aerodynamic performance, offering insight into how material deformation might be harnessed or mitigated in future aircraft design.

2 Objective

This lab was designed and conducted to examine how lift and drag vary with changes in angle of attack for wings made from materials with differing levels of flexibility. It also aimed to analyze the aerodynamic impact of wing deformation caused by material properties and explore how structural flexibility influences overall aerodynamic performance. In broader terms, this lab was intended to give the team a better understanding of the trade-offs between durability and aerodynamic efficiency when using flexible materials like TPU in wing design, which is critical for applications in small-scale or unmanned aerial vehicles.

3 Method

To complete this lab experiment, the Boeing Subsonic Wind Tunnel in ASL was used to test four different wing models in order of increasing ductility. These wings were mounted in the tunnel, then tested for a range of angles of attack from -4° to 16° in two-degree increments at 20Hz. LabVIEW software was used to record the lift and drag data for each test case.

3.1 Experiment Setup and Test Model(s)

This experiment was conducted in the Boeing Subsonic Wind Tunnel located in the Aerospace Sciences Laboratory near the Purdue University Airport. The wind tunnel includes a force balance system, a hot-film anemometer, and a Pitot-static probe for flow measurements. The test section has a transparent acrylic window for visualization and a mounting system for attaching various test articles to the internal force balance. For this experiment, the tunnel was operated at a fixed frequency of 20 Hz, providing a steady airflow for low-speed testing. Before testing, the tunnel was calibrated with no wing in place to zero the angle of attack and tare the forces. The interface in LabVIEW was used to monitor and record dynamic pressure, freestream velocity, and the lift and drag forces acting on each wing.

Each test run began with the wing set to an initial angle of attack of -4°, and the angle was increased in two-degree increments up to a maximum of 16°. At each step, data were recorded after flow stabilization. Between tests, the tunnel was powered down to allow for the safe removal and installation of the next test model. Figure 1 shows the wing mounted to pylons and actuator bar within the wind tunnel.

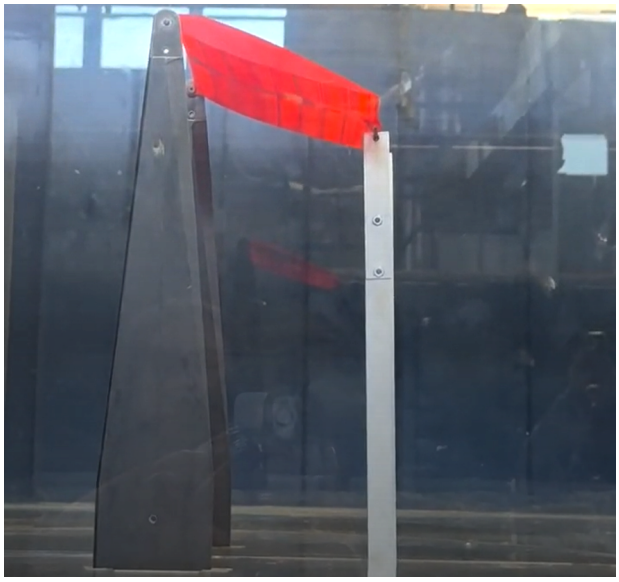

Figure 1: Finite wing mounted to pylons and actuator bar in Boeing wind tunnel

The existing tunnel structure and mounting hardware were left unchanged. The only modification to the setup was to mount each of the four custom, additively manufactured wing models properly. These were mounted on the same internal force balance mount used in previous labs via a two-rod horizontal attachment mechanism at the leading edge and a single attachment rod at the trailing edge, ensuring consistent alignment and structural support throughout all test conditions. The rod mounted at the trailing edge was adjustable and allowed for a varied angle of attack.

Figure 2: Finite wing of NACA 0012 profile, 8” chord, and 12” span

All wings were based on a NACA 0012 symmetric airfoil cross-section, chosen for its simple shape and aerodynamic properties. As shown in Figure 2, each wing had a chord length of eight inches and a span of 12 inches. Four different wings were tested, one brittle wing printed with PLA at 5% infill, and three flexible wings printed with TPU at varying perimeter thicknesses (1-3 wall loops) to control structural flexibility.

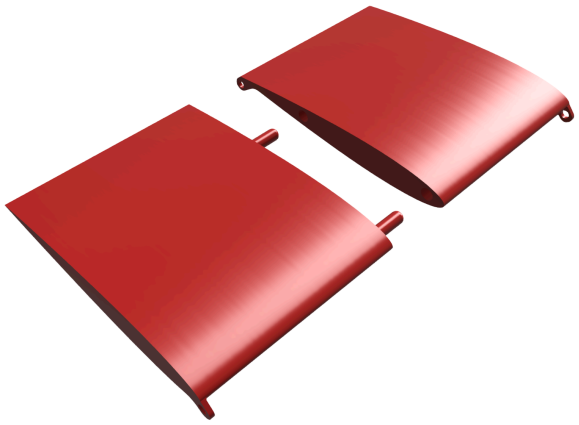

Figure 3: Separated finite wing sections (male/female halves)

Due to the build volume limits of the Bambu Lab A1 Mini 3D printer used in manufacturing, this wing had to be printed into two sections, as seen in Figure 3. The drawings and dimensions for these wing sections can be seen in Appendix A.

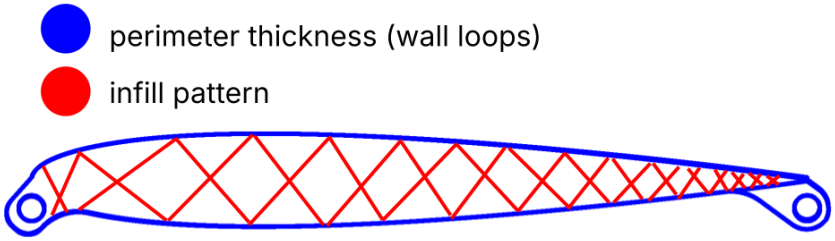

Figure 4: Infill propagation in additively manufactured wing

When additively manufactured, the wing’s cross-section is composed of the perimeter and the infill rather than being fully solid, demonstrated within Figure 4. The perimeter thickness is controlled by the number of wall loops set in Bambu Studio, varying from 1-3 for this experiment. The infill pattern utilized in Bambu Studio for this wing was “triangles,” which approximately propagates as shown in the diagram. The infill density, which dictates how thick the infill’s lattice spars are, was generally held constant at 5% for all wings except for the least flexible TPU wing, which had an infill density of 7%.

Model	Perimeter Thickness	Infill Density	Total Mass
Brittle	2 wall loops	5%	220.32 g
Least Flexible	3 wall loops	7%	276.40 g
Moderately Flexible	2 wall loops	5%	201.63 g
Most Flexible	1 wall loop	5%	145.89 g

Table 1: Summary of Bambu Studio slicer properties for each wing model

3.2 Instrumentation

The instrumentation used in this experiment was designed to accurately measure aerodynamic forces and flow properties within the wind tunnel. The primary tool for measuring lift and drag was the internal six-component force balance. To measure flow conditions, a hot-film anemometer was positioned downstream to provide a direct reading of the wind tunnel's airspeed.

All measurements, including lift, drag, angle of attack, dynamic pressure, and velocity, were recorded using a LabVIEW-based virtual interface. This software allowed us to capture and save data efficiently during each angle-of-attack increment. The angle of attack itself was controlled electronically using the tunnel's integrated motorized mounting system, which allowed precise adjustments in two-degree steps and included a zeroing feature to ensure consistent baseline orientation across tests.

3.3 Experimental Conditions

All tests were conducted at a constant wind tunnel frequency of 20 Hz, producing a steady airflow over the test wings. The airfoil was tested across a range of angles of attack from -4° to 16°, in 2-degree increments. The air density was assumed constant during the tests, based on ambient lab conditions. Each wing had the same geometry and was tested under the same flow conditions to isolate the effect of material flexibility on performance. The following table summarizes the key flow conditions:

Parameter	Value/Range	Notes
Tunnel Frequency	20 Hz	Constant for all tests
Freestream Velocity	12.37 m/s	Constant for all tests
Angle of Attack	-4° to 16°	2° increments
Air Density	1.23 kg/m^3	Assumed constant
Reynolds Number	170,000	Assumed constant

Table 2: Experimental Parameters

3.4 Procedures

The experiment began by logging into the lab computer and starting up LabVIEW. Next was the calibration of the wind tunnel's internal force balance system to ensure accurate force measurements. With the tunnel off and no test article mounted, we first tared the forces on LabVIEW and then performed a lift calibration by placing known weights onto the lift calibration plate. After each weight was added from 0.5 lbs up to 11.5 lbs, the corresponding lift force was recorded using the LabVIEW interface, and a linear calibration curve was created. This process was repeated for drag calibration. After collecting the calibration data, we fitted linear regression curves to both lift and drag plots. These calibration curves were used later to correct all measured force data.

With calibration complete, the tunnel was prepared for testing. A team member climbed into the test section to install the first wing model, starting with the brittle PLA wing, onto the force balance using the integrated rod mounting mechanism. The model was visually checked for alignment and secure placement before exiting the tunnel and lowering the door. Then, LabVIEW was used to adjust the angle of attack and set it to 0° using the "Zero AoA" button, and the system was tared once again.

Using the control panel, the tunnel was set to operate at 20 Hz, and the wind tunnel was turned on. The flow was allowed to stabilize before data collection began. For each test, the wing was evaluated at angles of attack ranging from -4° to 16°, in 2-degree increments. At each angle, the lift and drag readings were recorded using the LabVIEW interface, along with the dynamic pressure from the Pitot tube and velocity data from the hot-film anemometer. The "Push to Write" button was used to save each set of measurements. This data was then uploaded into Google Sheets for further calculations and analysis. After collecting data across the full angle range, the tunnel was turned off by using the control panel, and the angle of attack was reset to zero.

This procedure was repeated for all four test wings: one brittle PLA model and three flexible TPU wings with varying levels of perimeter thickness to alter material stiffness. Between each test, the tunnel door was raised and the previous model was replaced with the next. After completing all tests, the recorded data were corrected using the calibration curves, and the lift and drag coefficients were calculated. These were later used to create performance plots, such as lift coefficient versus angle of attack and drag polar curves. The lab was cleaned and reset to its original state before the team left.

4 Results

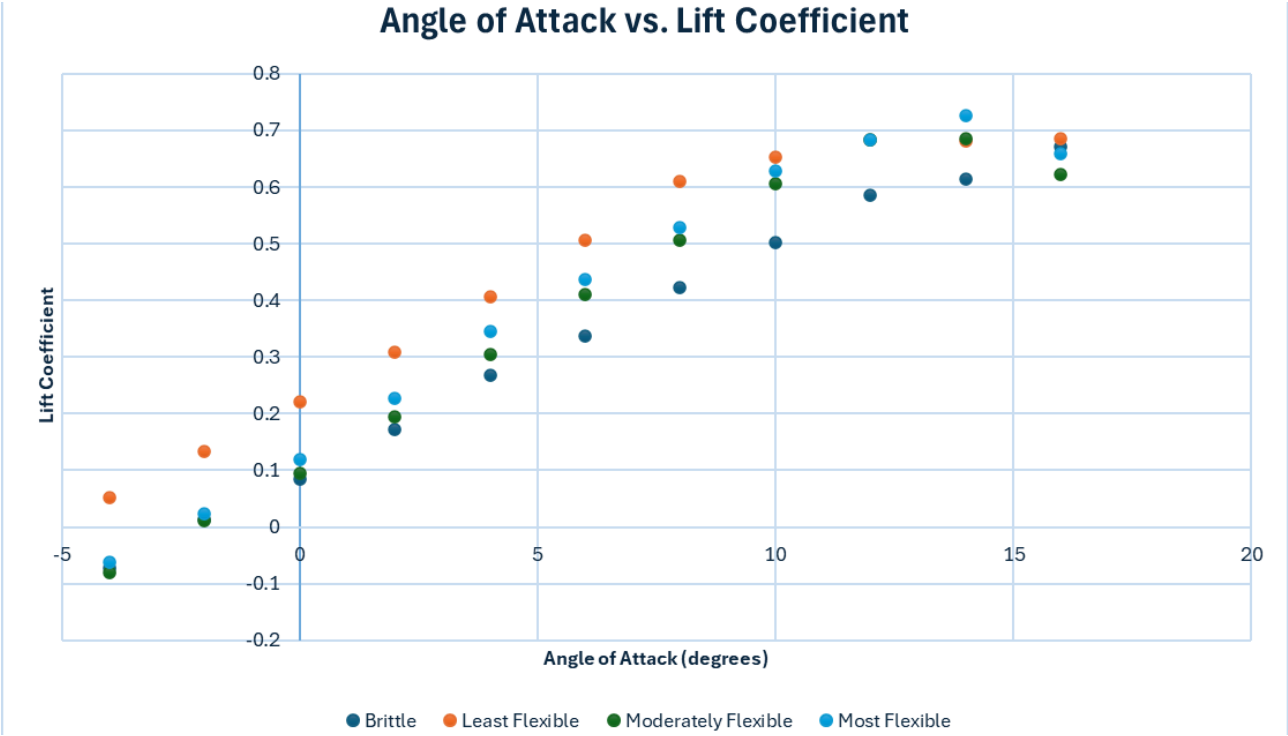

Figure 5: Angle of Attack vs Lift coefficient across all models.

The data compiled from lab experimentation is displayed in Figure 5. From the figure, there are a few significant trends, similarities, and discrepancies that can be observed between the datasets for each wing material. For the range of angles of attack between -4 to 10°, the relationship between lift coefficient and angle of attack is approximately linear for each wing. In this range, the least flexible wing has the greatest lift coefficient for a given angle of attack, followed by the most flexible wing, then the moderately flexible wing, and finally the brittle wing. At angles of attack above this range, the values reach a peak before dropping off at the upper limits of the angle of attack range for this experiment. During this phase, the most flexible

wing achieves the highest lift coefficient of any wing at any point in the figure at an angle of attack of 14 degrees.

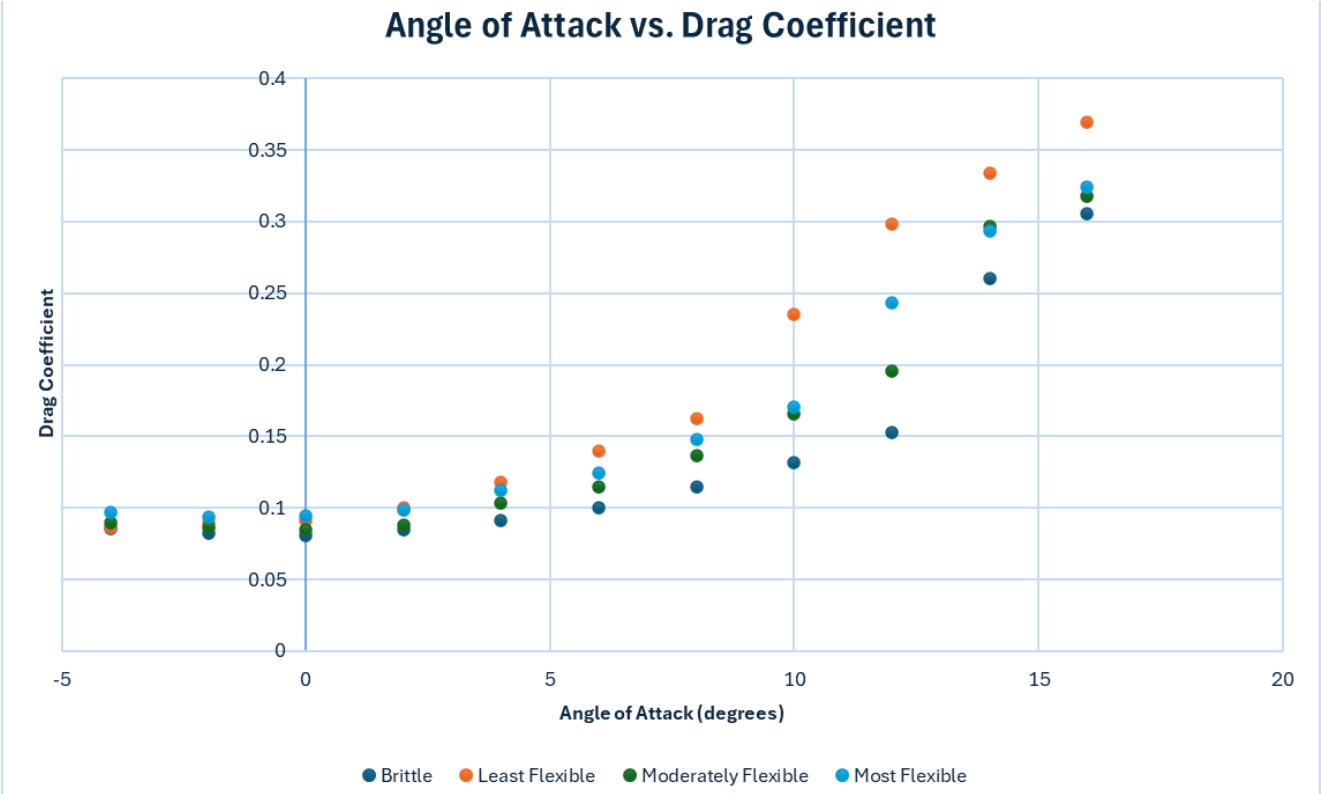

Figure 6: Angle of Attack vs. Drag Coefficient for all models.

In Figure 6, the drag coefficient trends of all four wings follow roughly the same curve for the whole range of angles of attack. The wings listed from greatest to least drag coefficient value for a given angle of attack are: least flexible, moderately flexible, most flexible, and brittle. At angles of attack below and up to 0 degrees, the drag coefficients for all four wings converge to similar values around just under 0.1.

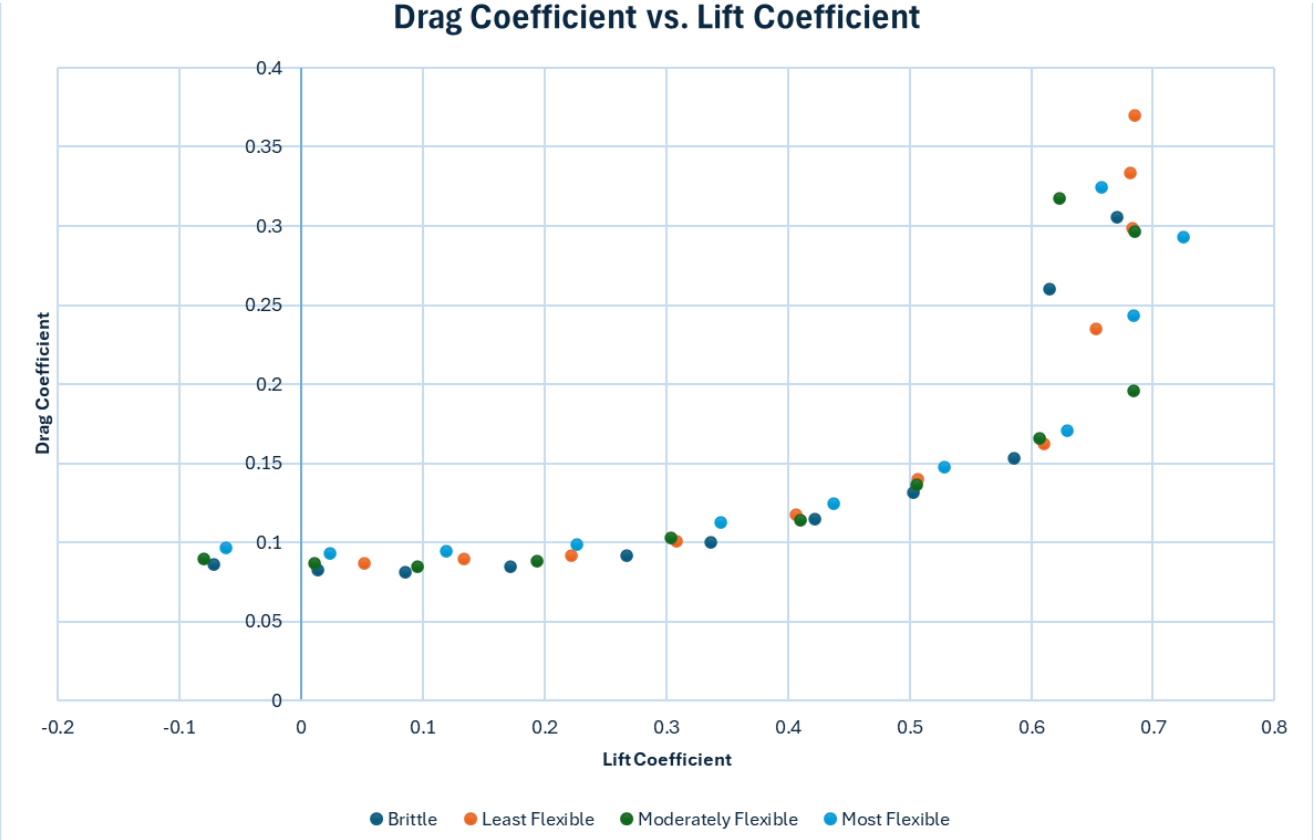

Figure 7: Drag coefficient vs Lift coefficient across all models.

Another figure to consider is the drag polar (Figure 7) for each wing. For coefficients of lift between -0.1 to 0.6, the drag polar curve is consistent and roughly the same for all four wings. At lift coefficients above 0.6, the relationship between drag and lift coefficients becomes unstable, with dramatic increases in drag coefficients and no discernible trends or comparable data between wings.

5 Discussion

The results from the experiment showed an unexpected trend compared to what was initially predicted. Data collected indicated that increasing wing flexibility produced higher maximum lift coefficients and lower drag coefficients. In addition to higher lift and lower drag, the results also showed that the more flexible wing had a higher stall angle as well, compared to a more brittle wing. This is the inverse of the initially predicted idea that lift would decrease while drag increased as the flexibility of the wing increased.

In addition to the proposed procedure at 20 Hz frequency, the most flexible wing model was tested at 35 Hz as well. In the 20 Hz test, this wing experienced fluttering at the trailing

edge corners for high angles of attack, which led to team interest in conducting an impromptu test at 35 Hz and 16° angle of attack.

Figure 8: Significant deformation of the most flexible wing model at 35 Hz testing frequency

At this higher frequency, the wing experienced significant fluttering at the trailing edge corners. In addition, there was an extreme amount of downwards deflection of the trailing edge corners at 35 Hz frequency, shown in Figure 8. This result aligns with the predictions from the finite element analysis shown in Figure 9, which indicates that maximum displacement occurs at each trailing edge corner.

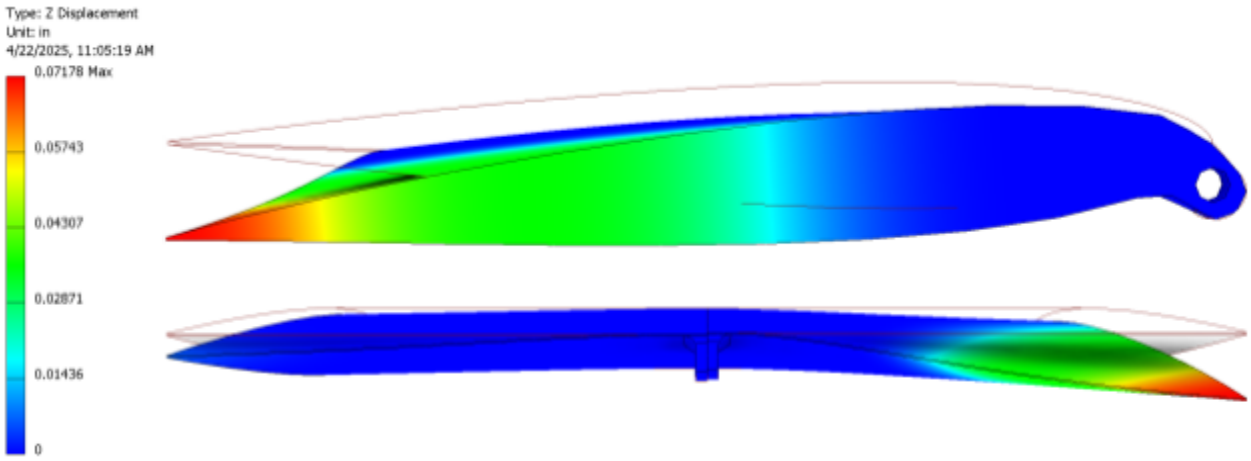

Figure 9: Trailing Edge Finite Element Analysis (Side and Back View)

This makes sense as the higher wind tunnel frequency has a major impact on the thin, highly ductile trailing edge corners of the wing. The fluttering of the trailing edge is similar to the actions of a mass-spring damper and can be explained in a similar way. Due to its flexibility, the aerodynamic forces acting on the wing caused the trailing edge to displace. At the same time, the elasticity resulted in a response displacement in the other direction, which in turn, created

oscillations in the form of flutter. Interestingly, however, the downwards deformation of the most flexible wing may have contributed to its high lift capabilities by effectively behaving like a deflected flap. From a design standpoint, this presents the possibility of intentionally deforming a flexible wing via internal actuators to perform the same behavior as control surfaces and high lift devices.

Concerning any limitations encountered throughout the experimental process, there were slight modifications made during the procedure to securely mount the wings in the wing tunnel. More specifically, while the leading edge of the wings were mounted using the pylons provided, the trailing edge mounting system did not align with the trailing edge of the wing. Therefore, it became necessary to use zip ties to secure the trailing edge pylon to the trailing edge of the wing. In the future, the lab technician should be consulted in the wing design procedure to ensure that the trailing edge is in alignment with the mounting device in the Boeing wing tunnel. Additional limitations include the roughness of the wing surfaces, which had the potential to cause surface drag throughout the experiment. Moving forward, care should be taken to remove any excess support material from the 3D-printed wings to test models that are as smooth as possible. Another possible solution to reduce surface drag would be to produce the wing models alternately with materials that can be safely sanded or smoothed down without risk of model integrity.

Overall, the objectives outlined in the Lab 6 Proposal were accomplished, and the experimental process ran smoothly with few minor issues throughout. The effect of wing flexibility on lift and drag was successfully tested for four separate models of increasing ductility at the proposed angle of attack range at 20 Hz in the Aerospace Sciences Laboratory’s Boeing wind tunnel.

References

1. Anderson, J. D. (2005). Ludwig Prandtl's boundary layer. Physics Today, 58(12), 42-48.

Appendix

Appendix A: Part Drawings of Models

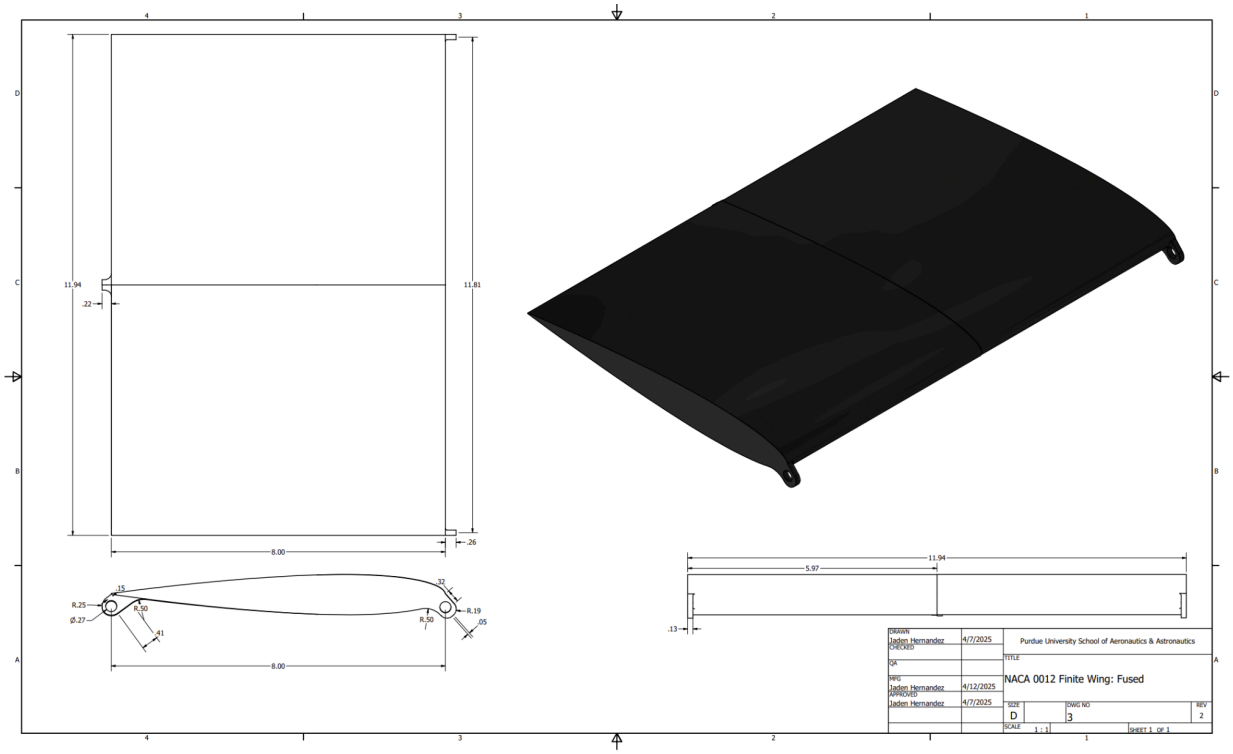

Figure 10: Finite Wing of NACA 0012 Profile, 8” Chord, and 12” Span Part Drawing

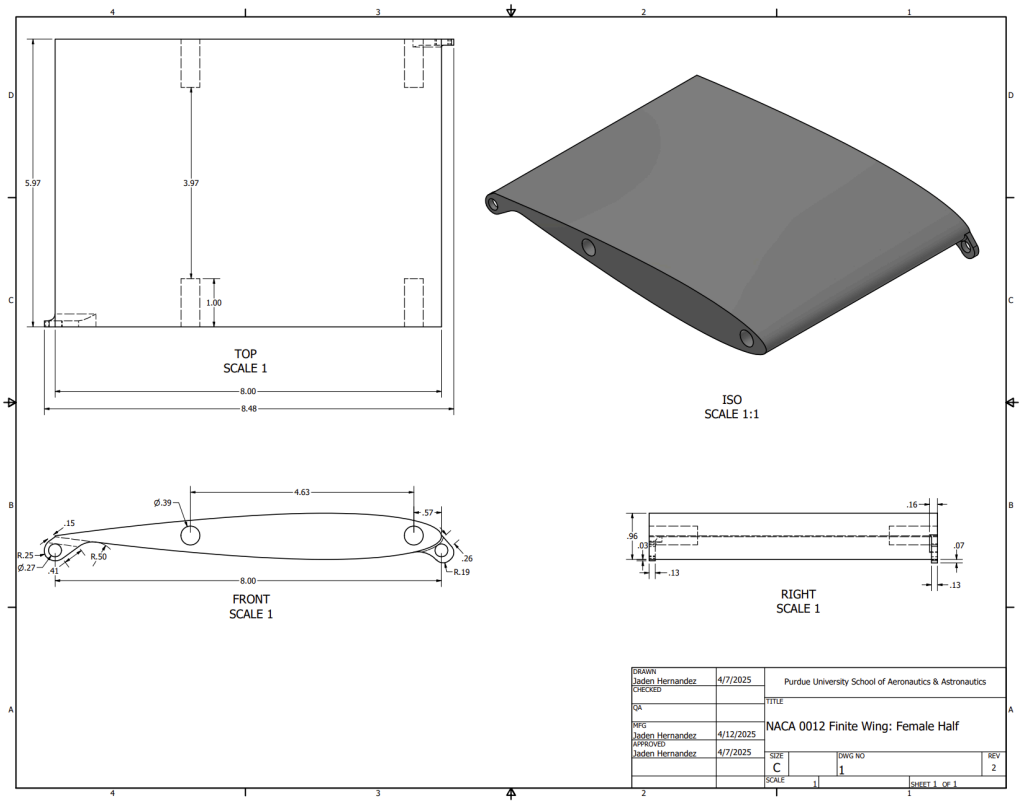

Figure 11: Female Wing Half of NACA 0012 Profile, 8” Chord, and 6” Span Part Drawing

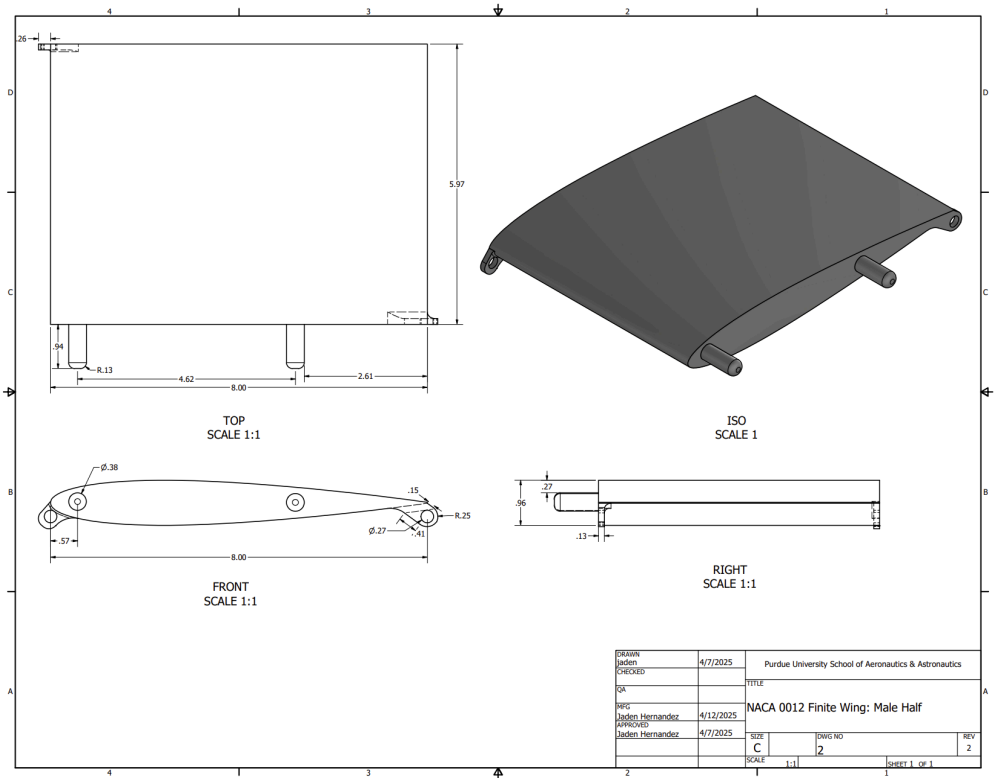

Figure 12: Male Wing Half of NACA 0012 Profile, 8” Chord, and 6” Span Part Drawing

Appendix B: Raw Data

Brittle Wing, English Units:

Angle of Attack (°)	Lift (lbs)	Drag (lbs)
-4	-0.09454134124	0.112602566
-2	0.0178313323	0.107704202
0	0.1117388332	0.106014777
2	0.2252017914	0.1113304669
4	0.3511060778	0.119836465
6	0.4406882185	0.1308147471
8	0.5532542782	0.1501790461
10	0.6592398809	0.172493132
12	0.7673141596	0.2002536948
14	0.8055228283	0.3408994501
16	0.8785570067	0.4004058527

Table 3: Lift and Drag Data for Brittle Wing

Least Flexible Wing, English Units:

Angle of Attack (°)	Lift (lbs)	Drag (lbs)
-4	0.06826136608	0.1135955783
-2	0.1757331571	0.1170981358
0	0.2909434869	0.1198280813
2	0.4037826683	0.1315990964
4	0.5324646199	0.1543811836
6	0.6634271919	0.1834501752
8	0.800182073	0.2129586632
10	0.8557390624	0.3083252928
12	0.8953154373	0.3910590544
14	0.8928972397	0.4371905313
16	0.8972502498	0.484382277

Table 4: Lift and Drag Data for Least Flexible Wing

Moderately Flexible Wing, English Units:

Angle of Attack (°)	Lift (lbs)	Drag (lbs)
-4	-0.1047751955	0.1173308323
-2	0.01442015891	0.1136261325
0	0.1249826055	0.1110608818
2	0.2542831646	0.1156324645
4	0.398025957	0.1350904756
6	0.5382032319	0.1497745753
8	0.6628106874	0.1788038836
10	0.7946529268	0.2174145498
12	0.8964319095	0.2563426818
14	0.8971846231	0.3885919871
16	0.8161161669	0.4158985215

Table 5: Lift and Drag Data for Moderately Flexible Wing

Most Flexible Wing, English Units:

Angle of Attack (°)	Lift (lbs)	Drag (lbs)
-4	-0.0805323498	0.1266884363
-2	0.03074814174	0.1223189958
0	0.1559539601	0.1233179699
2	0.2974187128	0.1290634684
4	0.4519812238	0.1471813786
6	0.5731314874	0.1629853652
8	0.6924685286	0.1934438287
10	0.8247222546	0.2234503134
12	0.8959346562	0.3193052516
14	0.950261838	0.3840589697
16	0.8623859799	0.4250260373

Table 6: Lift and Drag Data for Most Flexible Wing

Appendix C: Processed Data

Brittle Wing:

Angle of Attack (°)	Lift (N)	Drag (N)	Coefficient of Lift	Coefficient of Drag
-4	-0.4205198858	0.5008562134	-0.07214950511	0.08593298236
-2	0.07931376607	0.4790682907	0.01360803416	0.08219478139
0	0.4970143299	0.471553728	0.08527382211	0.08090549164
2	1.001697568	0.4951979167	0.1718634154	0.08496217617
4	1.561719834	0.5330325965	0.2679476451	0.0914535539
6	1.960181196	0.5818639952	0.3363125217	0.09983166246
8	2.46087503	0.6679963972	0.4222176442	0.1146095847
10	2.93229899	0.7672494512	0.5031008714	0.1316386456
12	3.413013382	0.8907284344	0.5855780779	0.1528242014
14	3.58296554	1.516320754	0.6147371368	0.260158427
16	3.907821566	1.781005233	0.6704733867	0.3055709146

Table 7: Lift and Drag Data for Brittle Wing

Least Flexible Wing:

Angle of Attack (°)	Lift (N)	Drag (N)	Coefficient of Lift	Coefficient of Drag
-4	0.3036265563	0.5052731322	0.05209386408	0.08669080265
-2	0.7816610826	0.5208525079	0.1341112803	0.0893637898
0	1.29411663	0.5329953054	0.2220343854	0.09144715579
2	1.796025309	0.585352781	0.3081479415	0.100430241
4	2.368402629	0.6866875047	0.4063519547	0.1178164584
6	2.950924149	0.8159863792	0.5062964302	0.1400005456
8	3.559209861	0.947240134	0.6106613235	0.1625200358
10	3.80632735	1.371430902	0.6530598048	0.2352993621
12	3.982363065	1.739430674	0.6832626328	0.2984378778
14	3.971606922	1.944623483	0.6814171781	0.3336432513
16	3.990969111	2.154532368	0.6847391907	0.3696577721

Table 8: Lift and Drag Data for Least Flexible Wing

Moderately Flexible Wing:

Angle of Attack (°)	Lift (N)	Drag (N)	Coefficient of Lift	Coefficient of Drag
-4	-0.4660400694	0.521887542	-0.07995950132	0.08954137283
-2	0.06414086683	0.5054090374	0.01100478706	0.0867141202
0	0.555922629	0.493998802	0.09538084623	0.08475644147
2	1.131051516	0.5143332021	0.1940569516	0.08824525842
4	1.770419457	0.6008824353	0.3037546902	0.1030946973
6	2.393927976	0.6661973108	0.4107313935	0.1143009116
8	2.948181937	0.7953196743	0.5058259429	0.1364547144
10	3.534616218	0.9670599175	0.6064417392	0.1659205588
12	3.987329133	1.140212249	0.6841146718	0.1956286783
14	3.990677204	1.728457158	0.6846891074	0.296555128
16	3.63008471	1.849916624	0.6228214745	0.3173941908

Table 9: Lift and Drag Data for Moderately Flexible Wing

Most Flexible Wing:

Angle of Attack (°)	Lift (N)	Drag (N)	Coefficient of Lift	Coefficient of Drag
-4	-0.3582078919	0.5635101647	-0.06145850172	0.09668265611
-2	0.1367677345	0.5440748934	0.02346553561	0.09334810463
0	0.6936832143	0.5485183303	0.1190167274	0.0941104747
2	1.322918435	0.5740743074	0.2269759732	0.09849516888
4	2.010412484	0.6546627719	0.3449308122	0.1123219058
6	2.549288856	0.7249589042	0.4373869953	0.1243827651
8	3.080100015	0.8604381502	0.5284594124	0.1476272319
10	3.668364588	0.9939069939	0.6293892359	0.1705267697
12	3.985117351	1.420269759	0.6837351915	0.2436787503
14	4.226764655	1.708294297	0.7251951415	0.2930957424
16	3.835892839	1.890515814	0.6581324196	0.3243598816

Table 10: Lift and Drag Data for Most Flexible Wing

APPENDIX D: SAMPLE CALCULATIONS

1. Calculation of Lift Coefficient

Example point: Brittle wing at angle of attack of 6 degrees

Lift is collected by the LabView software, and at this point the value is:

L = 0.44068821852 lbs

Now convert the lift value to Newtons by multiplying the pounds value by 4.448.

$$L_{Newtons} = 0.44068821852 * 4.448 = 1.960181196\ N$$

In order to calculate the lift coefficient from this, first find the dynamic pressure value using the following equation: $q_\infty = \frac{1}{2}\rho_\infty v_\infty^2 S$

From LabView, the anemometer wind speed value is 12.37 $\frac{m}{s}$. The density of air is 1.23 $\frac{kg}{m^3}$. The span of the wing is 0.3048 meters and the chord is 0.2032. Calculate the planform area, S.

$$S = b * c = 0.3048 * 0.2032 = 0.06194\ m^2$$

Now calculate dynamic pressure:

$$q_\infty = \frac{1}{2}\rho_\infty v_\infty^2 S = \frac{1}{2} * 1.23 * 12.37^2 * 0.06194 = 5.8289\ Pa$$

Now, use the following equation to calculate lift coefficient: $C_L = \frac{L}{q_\infty}$

$$C_L = \frac{L}{q_\infty} = \frac{1.960181196\ N}{5.8289\ Pa} = 0.33628664$$

The final lift coefficient is 0.336.

2. Calculation of Drag Coefficient

Example point: Brittle wing at angle of attack of 6 degrees

Drag is collected by the LabView software, and at this point the value is:

D = 0.1308147471 lbs

Now convert the drag value to Newtons by multiplying the pounds value by 4.448.

$$D_{Newtons} = 0.1308147471 * 4.448 = 0.5818639951\ N$$

Use the same dynamic pressure that was calculated in the lift coefficient section to calculate the drag coefficient using the following equation: $C_D = \frac{D}{q_\infty}$

$$C_D = \frac{D}{q_\infty} = \frac{0.5818639951\ N}{5.8289\ Pa} = 0.09982397967$$

The final drag coefficient is 0.099.

3. Calculation of Drag Polar

The calculation of lift over drag is very simple and requires one equation. To demonstrate this calculation, the same values as above will be used.

$$\frac{L}{D} = \frac{C_L}{C_D} = \frac{0.33628664}{0.09982397967} = 3.368796166$$

The value of lift over drag for this angle of attack is 3.369.